

## TOWARDS A FULLY COUPLED COMPONENT ZOOMING APPROACH IN ENGINE PERFORMANCE SIMULATION

Julien Pilet<sup>1,2</sup>, Jean-Loïc Lecordix<sup>1</sup>, Nicolas Garcia-Rosa<sup>2</sup>, Roger Barènes<sup>2</sup>, Gérard Lavergne<sup>2,3</sup>

<sup>1</sup>: Snecma, SAFRAN Group  
Engineering, Research & Technology  
77550 Moissy-Cramayel, France

<sup>2</sup>: Université de Toulouse, ISAE  
Propulsion Laboratory DAEP  
31055 Toulouse Cedex 4, France

<sup>3</sup>: ONERA/DMAE  
Aerodynamics & Energetics Modeling  
31055 Toulouse Cedex 4, France

### ABSTRACT

This paper presents a fully-coupled zooming approach for the performance simulation of modern very high bypass ratio turbofan engines developed by Snecma. This simulation is achieved by merging detailed 3D simulations and map component models into a unified representation of the whole engine.

Today's state-of-the-art engine cycle analysis are commonly based on component mapping models which enable component interactions to be considered, while CFD simulations are carried out separately and therefore overlook those interactions. With the methodology discussed in this paper, the detailed analysis of an engine component is no longer considered apart, but directly within the whole engine performance model. Moreover, all links between the 3D simulation and overall engine models have been automated making this zooming simulation fully-integrated. The simulation uses the PROOSIS propulsion object-oriented simulation software developed by Empresarios Agrupados for whole engine cycle analysis and the computational fluid dynamics (CFD) code CEDRE developed by ONERA for the high fidelity 3-D component simulations.

The whole engine model is created by linking component models through their communication ports in a graphical user-friendly interface. CFD simulated component models have been implemented in PROOSIS libraries already providing mapped components. Simple averaging techniques have been developed to handle 3D-to-0D data exchange. Boundary conditions of the whole engine model remain the same as for the typical 0-D engine cycle analysis while those of the 3-D simulations are automatically given by PROOSIS to CEDRE.

This methodology has been applied on an advanced very high bypass ratio engine developed by Price Induction. The proposed zooming approach has been performed on the fan stage when simulating Main Design Point as well as severe case of off-design conditions such as wind-milling. The results have been achieved within the same time frame of a typical CFD fully-converged calculation. A detailed comparison with upcoming test results will provide a first validation of the methodology and will be presented in a future paper.

### KEYWORDS

Gas Turbine, Zooming, CFD, Engine Performance, Engine test

### NOMENCLATURE

#### Acronyms

BPR	Bypass ratio
CFD	Computational Fluid Dynamics
FADEC	Full Authority Digital Engine Control
GT	Gas Turbine
HP	High Pressure
HPC	High Pressure Compressor
HPT	High Pressure Turbine
LP	Low Pressure
LPT	Low Pressure Turbine
MFT	Map Fitting Tool
OGV	Outlet Guide Vane

#### Latin letters

A	Area
At	Total sonic velocity
k	Turbulent kinetic energy
l	Turbulence integral length scale
M	Mach number
P	Pressure

r	Air gas constant
SE	Secondary map scalar for efficiency
SW	Secondary map scalar for mass flow
SX	Secondary scalar for rotational speed
T	Temperature
Ut	Velocity at tip
V	Velocity
W	Mass flow rate
XN	Shaft rotational speed (rpm)

#### Subscripts

s	Static conditions
a	Absolute
x	Axial
i	Localized value

#### Greek letters

$\alpha$	Absolute flow angle relative to engine axis
$\varepsilon$	Turbulent dissipation
$\pi$	Pressure ratio
$\eta$	Efficiency
$\rho$	Density
$\omega$	Specific dissipation rate
$\gamma$	Specific heat ratio
$\Omega$	Shaft rotational speed (rad/s)

## INTRODUCTION

The work presented in this paper is part of an ongoing PhD study led under a partnership between Snecma, one of the world leading manufacturers of aircraft and rocket engines, and the Aerodynamics Energetics and Propulsion Department (DAEP) of the French major aerospace engineering institute ISAE, in Toulouse. The first objective is to develop an efficient zooming methodology based on the coupling of engine cycle models and 3D CFD calculations, for the simulation of modern, very high bypass turbofan engine off-design performance. Then, this methodology will be validated with experimental tests at the DAEP bench. Finally, windmilling tests will be conducted to provide an original validation database in a severe case of off-design operation.

Coupled simulations are part of global collaborative research efforts that have been made to reduce development time and costs. A first 0-D/1-D zooming on a high-pressure compressor was achieved by Follen and auBuchon [1]. Different zooming approaches were also presented by an NTUA and NLR collaboration using a 1-D stage stacking code [2]. Turner et al. extended multi-fidelity zooming to a turbofan engine with component characteristics zoomed in partial performance maps for a 0-D cycle simulation [3]. A partially integrated approach to zooming was investigated using CFD for the intake at Cranfield University [4].

However, the previous efforts were limited either by the complexity of a full-engine simulation, the significant manual work for data exchange or CFD post-processing, or empirical correlations used in mean-line analysis most of which were validated near design point.

The numerical work undertaken focused on two axis of equal importance in order to achieve a significant step in zooming simulation: 1) off-design simulation at windmilling and 2) a fully coupled approach.

Therefore, at first, both the GT simulation tool PROOSIS and the CFD code CEDRE were validated for windmilling simulation. A full engine model of the DGEN 380 was created in PROOSIS using validated map components. The use of MFT extrapolated maps [5] allowed windmilling steady state to be reached and component behaviors to be well reproduced, even in such unusual very low speed zones where convergence problems are commonly encountered. It was also shown that compressors still compressed, but at a very low pressure ratio, and turbines would produce very little workload. Only the fan seemed to operate in a very different way as if it was “self-windmilling”.

From this observation, 3D analysis with CEDRE was performed on the fan stage and under windmilling conditions. At the same time, the zooming developments were carried out, only on the fan stage, but at design point for practical reasons. This phase defined specific strategies necessary for the coupling of the two codes and the methodology that will be applied in the beginning of 2011 for windmilling.

The work progress on the methodology of this PROOSIS-CEDRE component zooming approach applied on the DGEN 380 engine developed by Price Induction is described. Preliminary results proved the methodology to be promising. The paper also includes a presentation of the DGEN380 test rig at the ISAE Propulsion laboratory that will be used to provide significant test data for calibration and validation of the methodology starting from 2011.

## THE DGEN 380

The development of the methodology is carried out on an advanced very high bypass engine developed by Price Induction, the DGEN 380 (see Figure 1). It is a two spool unmixed flow geared turbofan jet engine designed for 2-6 seat light airplanes in a two engine configuration, for a maximum take-off weight between 1550 and 2550 kg. The DGEN 380 is optimized for a cruise altitude of 15000 ft and speed of Mach 0.338. The flight envelope extends operation up to 25000 ft and Mach 0.4.

Modern and performing materials such as composites and light alloys are used to achieve an optimized weight for components. The fan is less than 14 inches in diameter and consists of 14 blades, 40 for the OGV. The high pressure core consists of a centrifugal compressor and a single stage turbine. The low pressure turbine is also single stage. It is an all electric engine with an electric starter-generator system used to start the engine at any conditions and also, to power the regulation accessories for both oil and fuel systems. A FADEC electronic unit ensures general regulation.

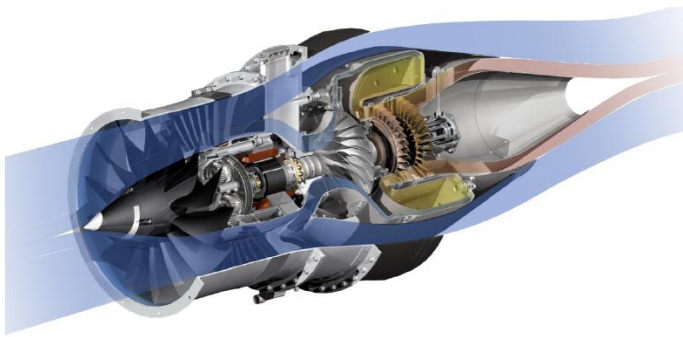


**Figure 1 : DGEN 380 engine architecture, courtesy of Price Induction**

The station nomenclature is presented in Figure 2. Additional stations are used to describe the zooming methodology and will be presented later on.

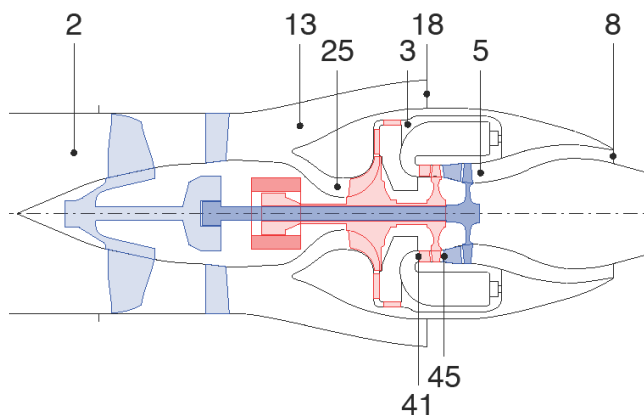


**Figure 2: stations nomenclature**

**PROOSIS**

The PPropulsion Object-Oriented SIMulation Software PROOSIS was developed by Empresarios Agrupados as part of the “VIVACE-ECP” project (Value Improvement through a Virtual Aeronautical Collaborative Enterprise - European Cycle Program). The Virtual Engine sub-project aimed at contributing to the reduction of lead time and development costs for a new or derivative gas turbine [1,6].

**Features and models**

PROOSIS is a modern and cost effective interactive gas turbine simulation software that not only offers core capabilities for engine performance modeling, such as:

- Conceptual engine designs,
- Steady, transient and off-design calculations,
- Single-point and multi-point design,
- Parametric studies,
- Sensitivity analysis,
- And customer deck generation;

but also advanced capabilities like multi-disciplinary modeling and zooming. The zooming functionality has previously been tested with a 1D stage stacking code [2].

PROOSIS primarily performs 0-D engine simulations based on the thermodynamic cycles of gas turbines, using averaged variables to describe the flow properties at the interface of component models. The individual component characteristics are given through maps obtained from CFD simulation or test results. The modeling of the fluid is determined by fluid and thermodynamic functions accordingly to the user’s state of the art. In this case, custom libraries developed for component models based on Snecma experience have been used instead of the standard libraries.

To calculate the performance at a specific operating point, PROOSIS solves a set of non-linear equations determined by the mass and power balance for all the components using a classical Newton-Raphson method. A second method known as the Broyden method [7,8] can be used to improve convergence speed.

**Component MFT maps**

The existing libraries provide map components that support both BETA and MFT formats. BETA is a well-known mathematical representation of components map used in many commercial GT software.

MFT or ‘Map Fitting Tool’ is a representation based on similarity parameters derived from the basic physics of the component. This type of representation was first explored by NASA and GE [5]. It was found that MFT maps were very accurate and resulted in smoother maps and meaningful extrapolation to regions not covered by initial data. All the performance maps used in the DGEN 380 model are of MFT type.

**The DGEN 380 PROOSIS model**

The user-friendly interface allowed a full model of the DGEN engine to be created easily and quickly using components from the existing libraries. Figure 3 shows the schematic view of the DGEN model in PROOSIS.

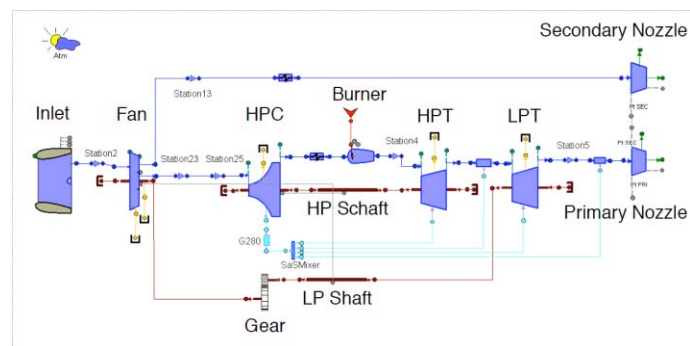


**Figure 3 : the DGEN 380 schematic in PROOSIS**

A simulation requires a partition to be created. A partition is a mathematical model generated by PROOSIS. Once the boundary conditions and iterative variables also called tearing variables of the model are defined by the user, PROOSIS automatically sorts the equations of the entire model to create the partition. Given the possibilities of boundary conditions and iterative variables, numerous partitions can be created and this will cause some difficulties in defining a general methodology for the zooming approach.

### Design Calculation

A design experiment was created in the wizard mode using the steady partition and additional closure equations that were input in order to perform a design at cruise conditions of 10'000 ft and Mach 0.338. This results in the tuning of secondary parameters in order to reach the exact specific thrust and fuel consumption at cruise of this engine using an analogue principle as described in [11].

These parameters are SE, SW and SXN calculated for each of the rotating components.

### Steady Calculation

The values previously determined in the design experiment for all the parameters listed were input in the component attributes. A steady experiment was created on the steady partition to run the cruise operating point and verify that the engine performance reached the expected values. This steady experiment was also used to run steady calculations at different operating conditions including far off-design. PROOSIS was able to simulate such a large envelope of conditions down to very low pressure ratios using the MFT maps.

Figure 4 shows the windmilling steady state area reached for different Flight Mach numbers in the fan map. Figure 5 and Figure 6 respectively plot the fan tip velocity to the inlet total sonic speed  $U_t/At_0$  and the flow parameter PHI versus for different Flight Mach numbers  $M_0$ . These results show that the fan speed is a linear function of  $M_0$  for the range simulated here.

Results also showed that power levels are several hundred times lower than at design point. The turbines produce little work: roughly 10 to 15% of the design work. The high pressure compressor operates at very low pressure ratio. The fan operates with a pressure ratio below 1 and with a very high BPR, more than 8 times higher than design values. Given the low power levels, the fan power equilibrium at windmilling seems to be driven only by the bypass.

All these results suggest that the fan is the most important component to simulate with CFD and that at a first step its analysis can be carried out separately from the other components as if the fan was "self-windmilling".

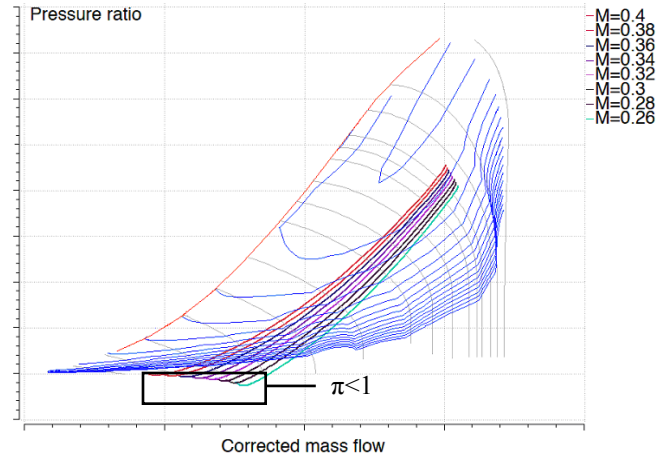


**Figure 4: fuel cut-off simulation and windmilling steady state for several Mach in the fan map**

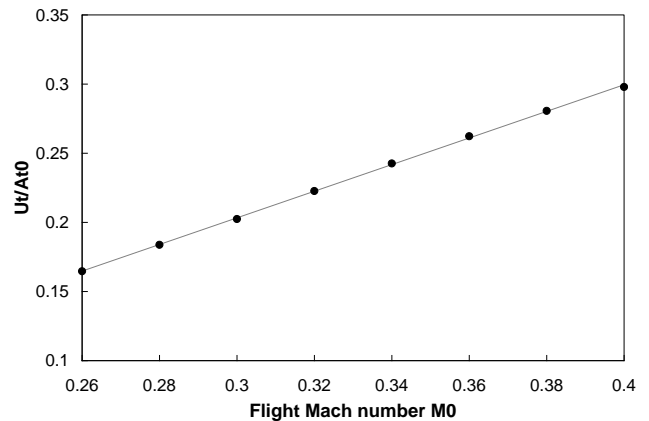


**Figure 5: fan rotational tip speed over inlet total sonic speed at windmill for several Mach**

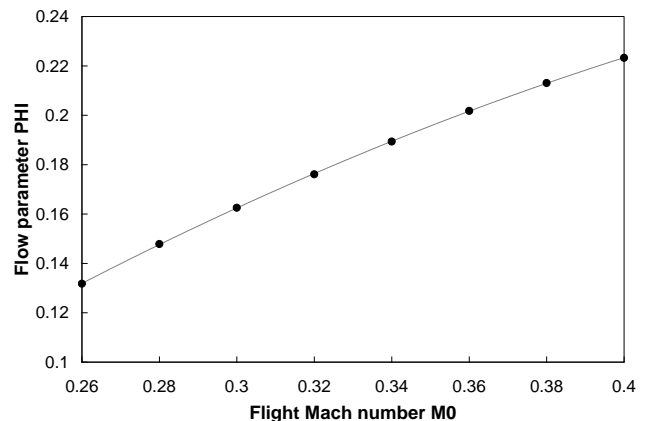


**Figure 6: flow parameter at windmill for several Mach, second order fitting**

## CFD CODE CEDRE

CEDRE is a powerful CFD code developed by ONERA [12] for multiphysics simulations for propulsion applications. It has proven to be particularly robust for very unadapted aerodynamic flows with large flow separations. The compressible flow module is used to solve the Reynolds Average Navier-Stokes equations for a periodic 3D domain.

Turbulence closure was achieved with a two-equation  $k$ - $l$  model by Smith [13,14]. The turbulent kinetic energy  $k$  transport equation is similar to the one in the more known  $k$ - $\epsilon$  and  $k$ - $\omega$  models. The difference lies in the second equation which is used to determine the integral length scale  $l$ .

The geometry studied, first separately, then in the zooming simulation, was available in a CAD format and is shown in Figure 7. It consists of the fan blade with the outlet guide vane which is located before the bypass, and the bypass itself. The design details of the geometry are property of Price Induction.

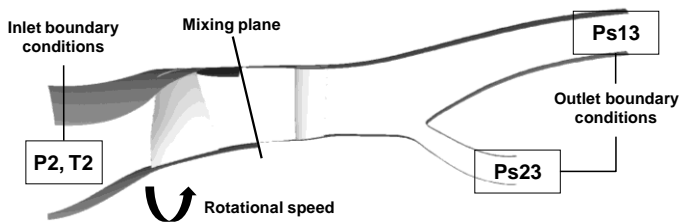


**Figure 7: Fan - OGV - bypass geometry**

The mesh was performed with Numeca's Autogrid 5 software. It is a classical 'o-4-h' structured hexahedric mesh for the fan and OGV blades and a 'c' mesh was used for the bypass, for a total number of cells of approximately 2.5 million. The fan is a  $20^\circ$  periodic sector and  $9^\circ$  for the OGV. During the pretreatment of CEDRE, the structured domains split into several computational domains for highly parallel calculations.

The boundary conditions used for all simulations are:

- static pressures  $Ps13$  and  $Ps25$  at the exit
- stagnation conditions at the inlet
- fan shaft rotational speed

In order to validate CEDRE for large flow separations, several simulations were run at near windmilling conditions using a technique that consists in iterating on boundary conditions until the spanwise aerodynamic load of the fan is zero. Simulations were first run on the fan blade alone, showing large separations near the tip. Adding the OGV blade and using the mixing plane technique for the fan and OGV interface had little effect on the flow across the fan.

The procedure to simulate windmilling for the entire geometry, as shown in Figure 7, consists in setting  $Ps13$  so that  $Ps18$  would equal the local ambient pressure and iterating on the fan rotational speed  $\Omega$  until the aerodynamic load of the fan

stage equaled zero.  $Ps25$  was then tuned in order to get the proper BPR.

Figure 8 shows the Mach number field in a blade-to-blade plane of the fan and OGV, achieved at windmilling for a fan rotational speed of 20% of design speed. The fan and OGV still behave properly at hub whereas separations appear at the tip, especially for the OGV. Further analysis on pressure profiles verified that the lower part of the fan blade compresses a little while the upper part expands the flow with an overall aerodynamic load of zero. These non-isentropic phenomena were expected [15] and proved CEDRE is able to simulate the flow path in severe off-design conditions.

However, this method requires to manually iterate on the rotational speed before reaching an overall load of zero. This is costly and inefficient compared to the zooming simulation where the fan boundary conditions are update within PROOSIS to satisfy power equilibrium on the low pressure core.

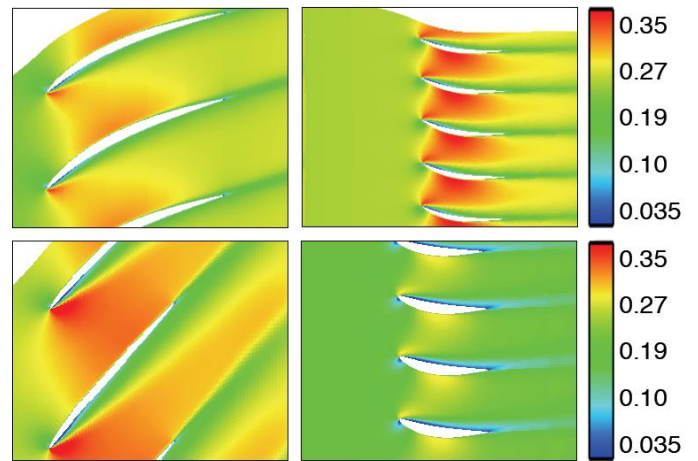


**Figure 8: Mach number on fan row (left) and OGV (right) – near hub (top) and near shroud (bottom) – at windmilling**

## ZOOMING METHODOLOGY

The methodology described in this paper does not calculate any mini-map for insertion in the usual 0-D model or any data for the 0-D model tuning with secondary scalars. It performs a single steady state simulation of the entire engine model in which 3D CFD simulations on a specific component are used as many times as required to reach full convergence, while other components still use the standard mapping models. This makes it a fully-coupled approach.

In order to make this methodology efficient and useful, a first requirement is to avoid systematic CFD simulations until convergence. Moreover, the approach needs to be fully-integrated as well as being fully-coupled. This implies that the entire process of CFD – pre-treatment, treatment and post-treatment – has to be automated. Boundary conditions must be automatically updated from the engine model to the CFD data

files and CFD results have to be post-processed to provide the expected feedback to the engine model. For this purpose, specific scripts have been developed and simple averaging techniques, inspired from the experience of Snecma, were implemented. It is important to note that the choice of averaging techniques can have a significant influence on the results and should be discussed in a specific paper.

Since the objective is to perform windmilling simulation, based on the previous remarks, the zooming is only carried out on the fan stage with the geometry defined in Figure 7. However the development of the methodology was performed at design point first, in order to address the difficulties of a CEDRE inclusion in PROOSIS before dealing with a far-off design case. The first difficulty of merging CEDRE into PROOSIS lies within the exit static pressures that are needed to run CEDRE with the boundary conditions defined in the previous section. Static pressure can be determined from stagnation pressure and temperature, mass flow and area. But the first three parameters are given by CEDRE within a global iteration and are therefore considered as unknowns at initialization. Additionally, the parameters provided to calculate the static pressure must be consistent with nozzle adaptation in the engine model. In an iterative process with partially converged CEDRE simulations, it is unlikely this condition is verified at all times. Therefore, strategies had to be developed first for the PROOSIS-CEDRE data exchange within the zoomed-in component, second the determination of CEDRE boundary conditions and the data exchange between the zoomed-in component and the other components within a given engine model in PROOSIS, and third, the iterative process.

The first step was to replace the fan component in Figure 3 with a new FanCEDRE component equipped with the same ports plus two extra static pressure ports at the outlet. This leads to a new schematic shown in Figure 9.

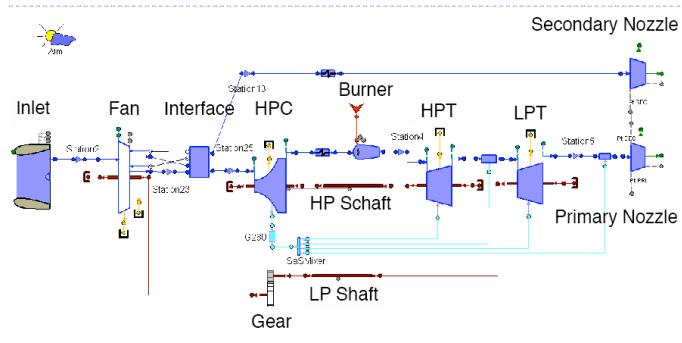


**Figure 9 : DGEN 380 schematic for zooming simulation**

PROOSIS can now provide the necessary boundary conditions, i.e. the rotational speed, inlet stagnation conditions and exit static pressures for CEDRE to calculate entry and exit mass flows and the exit stagnation conditions. This data exchange process is illustrated for the fan stage in Figure 10.

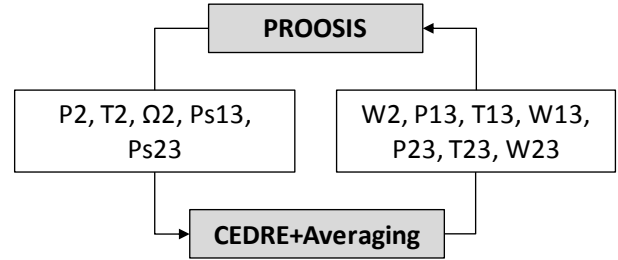


**Figure 10 : data exchange process between PROOSIS and CEDRE in the Fan component**

However, the acquisition of the exit static pressures is externalized from the fan component. This leads to the creation of a new component located after the fan in Figure 9, the Interface component. It is a key component in the zooming methodology: it not only calculates the exit static pressures but also manages the data exchange between the Fan component and the rest of the engine components. Moreover, the interface component breaks mass conservation. This last function is a mini-revolution in traditional cycle analysis in which mass balance is an important property of the flow physics modeling.

The nomenclature defined in Figure 11 will be used to reference the entry and exit stations of the interface component.

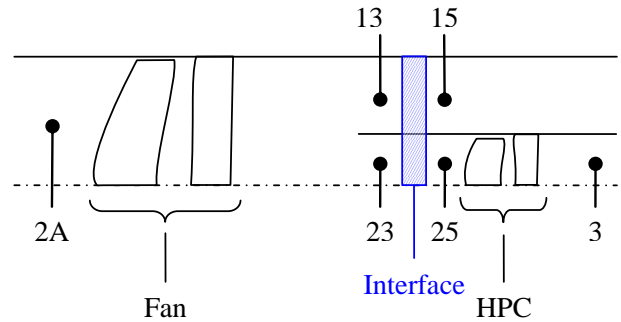


**Figure 11: stations and interface component locations**

The fluid properties across this component are given by equations (10), (11) and (12); total thermodynamic properties remain unchanged but the entry and exit mass flows do not match:

$$\begin{aligned} P_{13} &= P_{15} \\ P_{23} &= P_{25} \end{aligned} \quad (10)$$

$$\begin{aligned} T_{13} &= T_{15} \\ T_{23} &= T_{25} \end{aligned} \quad (11)$$

$$\begin{aligned} W_{13} &\neq W_{15} \\ W_{23} &\neq W_{25} \end{aligned} \quad (12)$$

W13 and W23 are calculated by CEDRE as described above and used in the power-balance equation of the LP shaft. W15 and W25 are determined differently and will only match W13 and W23 respectively when the simulation is converged, provided a minimum of thermodynamic consistency is achieved in the different processes and the averaging techniques.

As mentioned above, nozzle adaptation cannot be verified for any random value of the (P,T,W) 3-tuple. PROOSIS detects a conflict in the engine model equations between assigned values of P,T and W and nozzle adaptation and therefore cannot create a partition: the breaking of mass conservation is a mean to overcome this difficulty.

Static pressure Ps13 is determined using total quantities P13, T13, area A13 and mass flow W15. Similarly, Ps23 uses P23, T23, area A23 and mass flow W25. These are the static pressures sent to the fan component to perform the CEDRE simulations.

Mass balance being broken only locally at the interface component, W15 and W25 are equal to W18 and W8 respectively, minus the fuel injection contribution in mass flow for the primary flow. Whereas W13 and W23 cannot be determined for nozzle adaptation using mass balance principle and total properties P13, T13 and P23, T23 respectively, W18 and W8 can. Therefore, the interface allows CEDRE simulations to be run with the necessary boundary conditions and the update of these conditions with the simulation results. This process illustrated in Figure 12 is iterated on until full convergence is reached, taking into account interactions between components at every step in CEDRE simulations as it usually does in full map models.

The dashed arrow pointing at “Nozzles” in Figure 12 means the data in stations 15 and 25 are altered by the other components located upstream of the nozzles. The differences between values at stations 15 and 18, and 25 and 8 respectively, are of no importance regarding this boundary conditions acquisition process. The dashed one leaving the W18 and W8 mass flows box is to remind that W18 and W8 are not directly used by the interface to determine the static pressures but because of mass conservation between 15 and 18, and 25 and 8 respectively, it is equivalent.

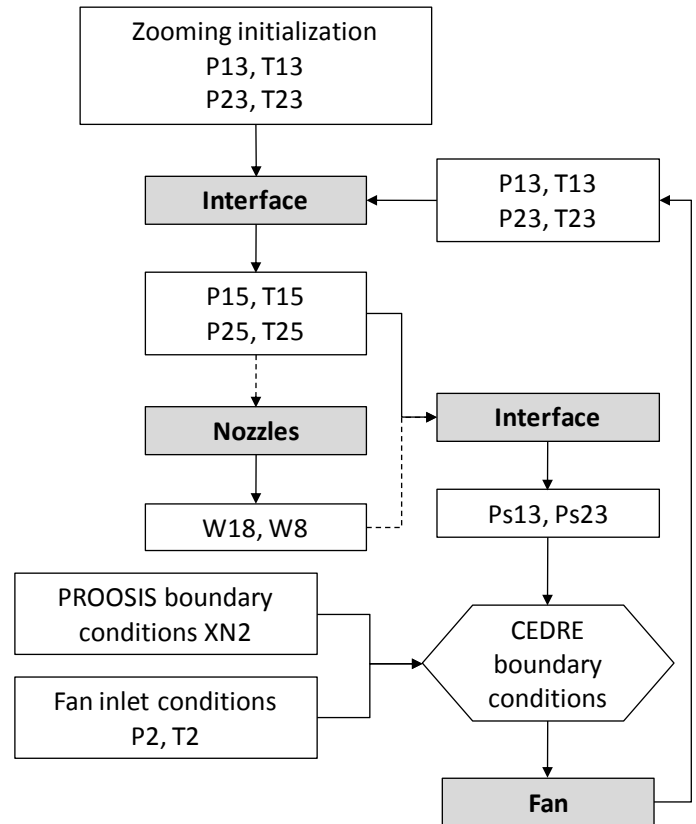


**Figure 12 : Fan exit boundary conditions acquisition process**

The difficulty is to control this iterative process for two main reasons: first, because there are as many patterns as there are partitions and second, because convergence depends on the options chosen for the PROOSIS solver. Indeed, the partition diversity problem has already been mentioned and choosing to run the simulation with or without the Broyden method completely changes the convergence sequence. Trying to solve the equations directly or improving the initial guess of the iterative variables first are also two different options that impact the convergence sequence.

In a decoupled or semi-coupled approach, the launch sequence of 3-D simulation has to be explicitly given. But in this fully-coupled approach, the sequence is not determined by the user but by PROOSIS solver. Indeed, CEDRE can be seen as a PROOSIS subroutine called when needed by PROOSIS solver to improve the residues calculated for the iterative variables defined in the partition. However, it would be highly inefficient to run CEDRE at every PROOSIS iteration. For this reason, it was chosen to use the Broyden Method mentioned in the PROOSIS section. The algorithm is presented in Figure 13.

With this algorithm, a CEDRE simulation is launched every time PROOSIS solver goes through the outer loop and the Jacobian matrix evaluation. At this stage, it will run the fan

boundary conditions acquisition process of Figure 12 and then perform Figure 10.

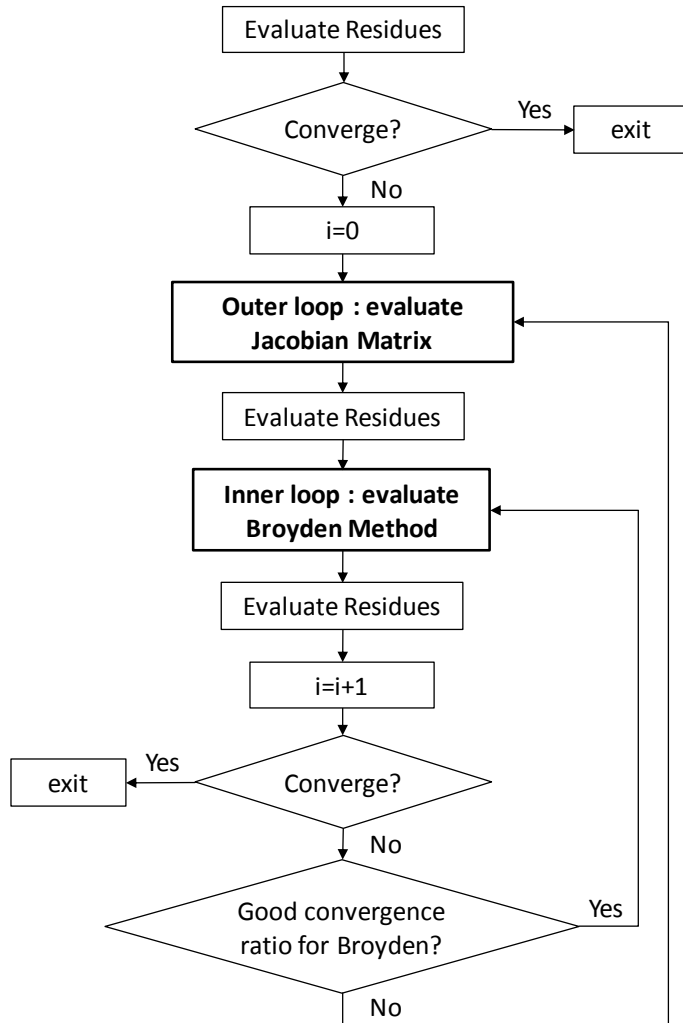


**Figure 13 : PROOSIS solver algorithm**

However, this is not run indefinitely: the iterative process between PROOSIS and CEDRE must be interrupted by user-defined criteria. For example, conditions on CEDRE return can be used to determine whether another 3D simulation is necessary or not.

### ZOOMING PRELIMINARY RESULTS

The zooming methodology presented here above has been tested with a partition using the fan shaft rotational speed XN2 as a boundary condition. This means XN2 remains constant throughout the entire simulation. Each CEDRE simulation consists in 200 iterations. The zooming calculation was run at design conditions to validate the methodology. Simulations results are presented in Figures 14, 15, 16, 17, 18 and 19:

- Figures 14, 15 and 17 show respectively total and static pressures, total temperatures and mass flows at the fan

interface after each PROOSIS-CEDRE iteration. Only six PROOSIS-CEDRE iterations were needed to reach convergence and Figure 15 shows that mass balance is achieved by then even though it was broken in the interface component.

- Figure 16 is a histogram plotting relative variations of total and static pressures and mass flows at stations 13 and 23 between two consecutive PROOSIS-CEDRE iterations  $i+1$  and  $i$  marked as  $\Delta i+1,i$ . This relative variation of a parameter  $X$  is given in percentage by:

$$\Delta X = \frac{X_{i+1} - X_i}{X_i} \cdot 100$$

Bars are considerably lower at  $\Delta 6,5$  than at  $\Delta 2,1$  meaning the entire process is stabilizing and rather quickly. Figure 15 also shows that the primary flow requires more time to stabilize.

- Figure 18 shows the variation of the fan exit mass flows in PROOSIS (W15 and W25) and in CEDRE (W13 and W23) in a CEDRE iteration time frame, scale is in thousands. Exit static pressures Ps13 and Ps23 are also plotted in Figure 17 on a secondary axis to simultaneously show the CEDRE boundary conditions update by PROOSIS after each PROOSIS-CEDRE iteration.

- Figure 19 is a histogram plotting the percentage of relative variations of mass flows between stations 13 and 15, and 23 and 25 respectively, after each PROOSIS-CEDRE iteration:

$$\Delta W_{13,15} = \frac{W_{13} - W_{15}}{W_{15}} \cdot 100$$

$$\Delta W_{23,25} = \frac{W_{23} - W_{25}}{W_{25}} \cdot 100$$

PROOSIS-CEDRE iteration 0 means no CEDRE simulation has been performed. Therefore, mass flows W2, W13 and W23 don't have any value yet. However, at the start, PROOSIS is initialized with stagnation pressures and temperatures P13, P23 and T13, T23 on top of the iterative variables of the model used in PROOSIS solver. Consequently, initial values of mass flows W15, W25 and static pressures Ps13, Ps23 can be calculated with the boundary acquisition process from Figure 12. All these values are plotted on Figures 14, 15 and 17. PROOSIS-CEDRE iteration 0 was also required to set meaningful flow properties throughout the meshed geometry before starting the actual simulation. The boundary conditions used for this first simulation are passed from PROOSIS to CEDRE using PROOSIS initialization. These are given either by previous steady PROOSIS simulations using the MFT maps for all components or by test data.

As can be seen in Figure 18, the primary axial velocity is negative during the first 300 iterations and as a result, so would

the primary flow be. This is unacceptable for PROOSIS: mass flows must be positive. Since simulations were launched on a 200-iteration basis, it took 400 iterations for this simulation to settle a meaningful positive flow both in primary and secondary channels.

The reason for this negative flow is that initial exit static pressures Ps13 and Ps23 given by PROOSIS are higher than the homogenous pressure (near P2) used to initialize the geometry with CEDRE (see Figure 14 for pressures). Therefore, during the first iterations, the compression across the fan blade is not established yet and the pressure being higher downstream, the flow is reversed. This was only observed for the primary flow because the secondary static pressure, being closer to the initial pressure, even though higher, is less disturbed by reverse flows. In fact, the secondary flow is more affected by what is happening in the primary and suffers the addition of the primary reverse flow with the flow coming from the inlet.

Figure 14 shows that the pressure rise is obtained progressively as the static pressures stabilize. The convergence criterion mentioned in the previous section calculates the relative difference of secondary stagnation pressure P13 after two consecutive CEDRE simulations ( $\Delta P13$ ); if it is below a predefined value, then the zooming is considered as converged. This value must be chosen carefully to filter boundary conditions fluctuations that do not affect CEDRE CFD results anymore. To establish a pertinent value for the results presented in this paper, separate CEDRE simulations were run for a wide range of boundary conditions. Also, the zooming was performed with different values for the criterion and it was obvious that below a certain point, it would have been useless to continue to perform CEDRE simulations. This was made to validate the methodology and criteria used along.

Figure 15 shows that temperature variations are not very important compared to pressure variations meaning mass flows W15 and W25 depend mainly on pressure. After the first PROOSIS-CEDRE iteration, total pressures P13 and P23 drop (Figure 14) causing W15 and W25 to follow (Figure 18). However, W13 and W23 calculated by CEDRE are lower than W15 and W25 for the exact same total pressures. In order to increase W13 to W15 level and W23 to W25 respectively, Ps13 and Ps23 have to be diminished at iteration 2 (Figure 14).

With these adjustments at iteration 2, P13 rises whereas P23 continues to drop. Simultaneously, W13 rises significantly, surpassing W15. Therefore, Ps13 has to be increased at iteration 3. But  $\Delta W13,15$  being lower at iteration 2 compared to iteration 1 (Figure 19),  $\Delta Ps13$  is lower at  $\Delta 3,2$  than at  $\Delta 2,1$  (Figure 16). In the primary flow, both W23 and W25 decrease (Figure 17) and since  $\Delta W23,25$  has also increased (Figure 19), the adjustment is more brutal causing Ps23 to decrease even more at iteration 3 (Figure 14).

Iteration 3 shows a rise in both P13 and P23 (Figure 14) and consequently of W15 and W25 (Figure 17). W13 and W23 have also increased getting closer to W15 and W25:  $\Delta W13,15$

and  $\Delta W23,25$  have decreased in norm between PROOSIS-CEDRE iterations 2 and 3 but are both positive (Figure 19). Therefore, both Ps13 and Ps23 increase at iteration 4 (Figure 14):  $\Delta Ps13$  and  $\Delta Ps23$  positive at  $\Delta 4,3$  in Figure 15.

From iteration 4 onwards,  $\Delta W13,15$  and  $\Delta W23,25$  are significantly lower (Figure 19) and  $\Delta P13$  and  $\Delta P23$  are less than 0.1% in norm at  $\Delta 5,4$  and  $\Delta 6,5$  (Figure 16). This means that total pressure rise is achieved and the last PROOSIS-CEDRE iterations are simply static pressure adjustments to achieve mass balance. These adjustments are small:  $\Delta Ps13$  and  $\Delta Ps23$  less than 0.2% in norm at  $\Delta 5,4$  and  $\Delta 6,5$  (Figure 16).

Table 1 below gives a comparison of overall performance in relative difference between the full MFT-map engine model and the PROOSIS-CEDRE model.

XN2	XN25	W2A	Fan $\pi$	Fan $\eta$	BPR	Thrust
0.0%	0.26%	-0.74%	0.1%	0.13%	-0.71%	-0.76%

**Table 1 : performance comparison between full MFT PROOSIS simulation and PROOSIS-CEDRE zooming simulation**

Given the simplification used for this first zooming simulation, results are quite satisfying. The difference between the traditional MFT model and the zooming model can be explained by the difference of methodology in the simulations that determined the fan map and the fan zoomed-in performance.

## THE DGEN 380 TEST BENCH

A DGEN 380 test bench has been installed at the propulsion laboratory of ISAE. A thorough work has been done to prepare the bench for both near design point and off-design tests. The tests are scheduled for the first quarter of 2011. The aim is to provide all the validation data for the numerical work presented until now. This will help design, calibrate and initialize parameters for all the engine models.

The engine test bench is equipped with two sets of sensors of different range in order to detect the smaller pressure fluctuations encountered at off-design or low speed regions. Temperatures and shafts mechanical speeds will also be monitored.

A special attention was brought to the Fan-OGV and bypass area. A major objective is to accurately qualify the flow path for very different speeds.

Intrusions in the vane with Prandtl, Pitot, three- and five-hole pressure probes have been prepared at several stations: upstream of the fan, in between the fan and OGV rows, right after the OGV and very close to the bypass nozzle as drawn on Figure 20. The Pitot and Prandtl probes allow static pressures to be measured and a first estimation of the mass flow using the total pressure information. Hot wires will be used at windmilling for velocity profiles in order to give a second more

accurate estimation of the mass flows and provide comparison with other measurements. A system is being developed to measure velocities at the exit of both primary and secondary nozzle.

Pressure combs have also been placed at strategic locations to provide measure comparisons. Station 2 is equipped with three radial pressure combs at 60 degrees from each other. Each probe has five holes with same radial spacing that can provide pressure profiles with averaged values of the holes located on a same area-ring.

Behind the OGV, there are four pressure combs of eight holes each. Finally, station 5 is equipped with three four-hole pressure combs.

The electric starter-generator system will be used as both a starter providing energy and power to the high pressure core, and a generator taking power off from it. This will allow studying the engine behavior and performance in windmilling for various engine loads.

## CONCLUSIONS AND FUTURE WORK

A first 0-D/3-D fully-coupled zooming approach was developed in the Snecma computer environment and has been applied on the DGEN 380 very high bypass engine.

3D CFD simulations were performed on the fan stage using CEDRE. Separate simulations were run to validate the code for simulating Main Design Point as well as far off-design conditions such as wind-milling before running coupled simulations.

In the zooming approach, CFD results were exchanged directly with the other components in the engine model within the PROOSIS environment. The partition used is well-adapted for cases where the fan rotational speed is known because the number of CEDRE unknown boundary conditions then drops by one. It will also be very adapted for the off-design simulations with test data input.

In 2011, the test bench at ISAE Propulsion lab will provide significant rig data that will help calibrate and validate the engine performance model and zooming simulations. The work on the zooming methodology will continue in order to improve its robustness and flexibility. The zooming may be extended to other components like the high pressure compressor. Thermodynamic consistency between PROOSIS and CEDRE will be improved with more accurate averaging techniques and their influence on simulation results studied. CEDRE initialization will be improved making use of the first iterations to start convergence in the same process. Finally, impact of mesh density should also be evaluated.

## ACKNOWLEDGMENTS

The authors would like to express their sincere gratitude to Snecma for its financial support and for authorizing the publication of the present paper. Special thanks to Snecma experts for their help and advice with CEDRE and PROOSIS.

We would also like to thank the technical team at ISAE Propulsion laboratory for helping set up the DGEN test bench, Price Induction for providing us with support and engine data. Finally, we would like to thank Empresarios Agrupados and ONERA support teams for their help and solution on specific questions.

## REFERENCES

- [1] G. Follen, M. auBuchon, "Numerical Zooming Between a NPSS Engine System Simulation and a One-Dimensional High Compressor Analysis Code", NASA-TM-209913, 2000
- [2] A. Alexiou, E. H. Baalbergen, O. Kogenhop, K. Mathioudakis, P. Arendsen, "Advanced Capabilities for Gas Turbine Engine Performance Simulations". Proceedings of ASME Turbo Expo 2007, Power for Land, Sea, and Air, May 14-17, 2007, Montreal, Canada
- [3] Mark G. Turner, John A. Reed, Robert Ryder, Joseph P. Veres, "Multi-Fidelity Simulation of a Turbofan Engine with Results Zoomed into Mini-Maps for a Zero-D Cycle Simulation". Proceedings of ASME Turbo Expo 2004, Power for Land, Sea, and Air, June 14-17, 2004, Vienna, Austria
- [4] V. Pachidis, P. Pilidis, G. Guindeuil, A. Kalfas, I. Templalexis, "A partially integrated approach to component zooming using computational fluid dynamics". Proceedings of ASME Turbo Expo 2005, Power for Land, Sea, and Air, June 6-9, 2005, Reno-Tahoe, Nevada, USA
- [5] G.L. Converse and R.G. Giffin, "Extended Parametric Representation of Compressors Fans and Turbines Vol. I – CMGEN User's Manual". NASA-CR-174645, March 1984, Cincinnati, Ohio, USA
- [6] Vivace Public Presentation, January 2006.
- [7] Pedro Cobas, "Numerical Algorithms in PROOSIS/Ecosim Pro", EAI Document, June 2010
- [8] C. G. Broyden, "A Class of Methods for Solving Nonlinear Simultaneous Equations", Mathematics of Computation (American Mathematical Society), Vol. 19, No. 92, October 1965
- [9] A. Alexiou, K. Mathioudakis, "Gas Turbine Engine Performance Model Applications Using an Object-Oriented Simulation Tool". Proceedings of ASME Turbo Expo 2006, Power for Land, Sea, and Air, May 8-11, 2006, Barcelona, Spain
- [10] S. Pakanati, R. Sampath, R. Irani, R. C. Plybon, B. A. Anderson, "High Fidelity Engine Performance Models For Windmill Relight Predictions". AIAA 2006-4970, 42<sup>nd</sup> AIAA/ASME/SAE/ASEE Joint Propulsion Conference & Exhibit, July 9-12 2006, Sacramento, California, USA
- [11] A. Alexiou, K. Mathioudakis, "Development of Gas Turbine Performance Models using a Generic Simulation Tool", Proceedings of ASME Turbo Expo 2005, Power for

Land, Sea, and Air, 6-9 June 2005, Reno-Tahoe, Nevada, USA

- [12] P. Chevalier, B. Courbet, D. Dutoya, P. Klotz, E. Ruiz, J. Troyes, P. Villedieu, "Cedre: Development And Validation Of A Multiphysic Computational Software". European Conference for Aerospace Sciences, EUCASS 2005, Moscow, Russia, 2005.
- [13] B.R. Smith, "The k-kl Turbulence Model and Wall Layer Model for Compressible Flows", 21<sup>st</sup> AIAA Fluid Dynamics Conference, paper 90-1483, June 18-20, 1990, Seattle, Washington, USA
- [14] B.R. Smith, "A Near Wall Model for the k - I Tho Equation Turbulence Model", 25<sup>th</sup> AIAA Fluid Dynamics Conference, paper 94-2386, June 20-23, 1994, Colorado Springs, Colorado, USA
- [15] D. Prasad, W. K. Lord, "Internal Losses and Flow Behavior of a Turbofan Stage At Windmill", Proceedings of ASME Turbo Expo 2008, Power for Land, Sea, and Air, June 9-13, 2008, Berlin, Germany
- [16] J. J. More, B. S. Garbow, K. E. Hillstrom, "User Guide For MINPACK-1". Applied Mathematics Division, Argonne National Laboratory, 9700 South Cass Avenue, IL 60439

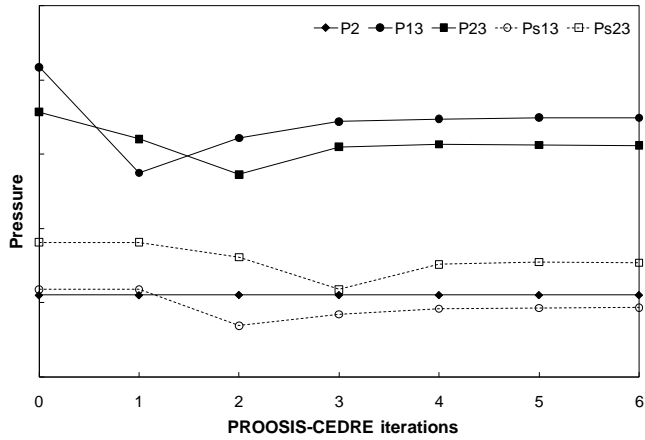


Figure 14: Fan static and stagnation pressures at the end of each PROOSIS-CEDRE iteration (design point)

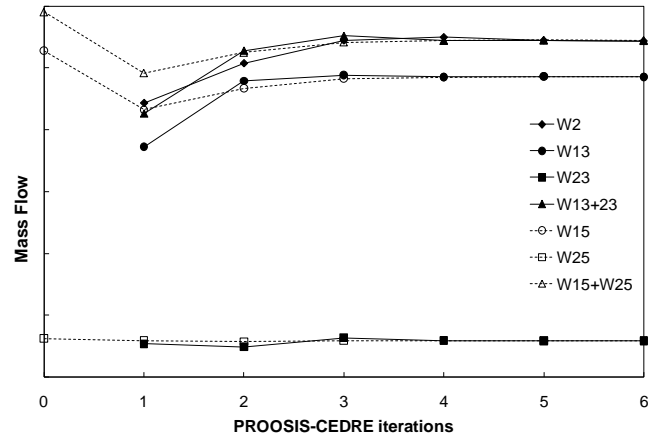


Figure 17: Fan mass flows at the end of each PROOSIS-CEDRE iteration (design point)

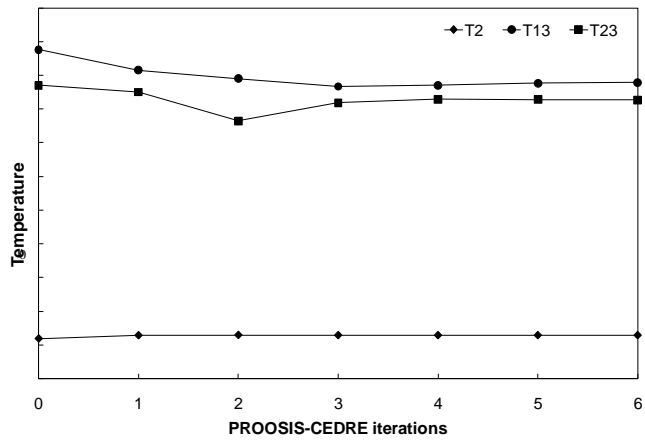


Figure 15: Fan stagnation temperatures at the end of each PROOSIS-CEDRE iteration (design point)

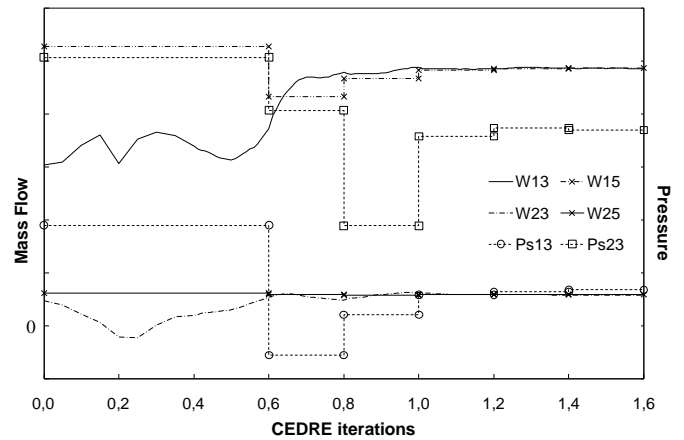


Figure 18: Mass flow variations and CEDRE exit boundary conditions during the entire simulation (design point)

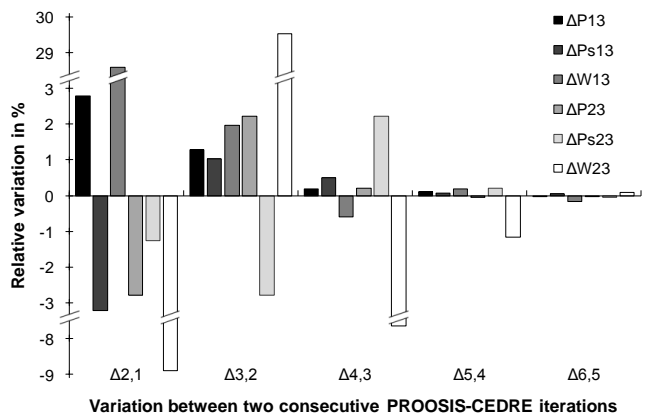


Figure 16 : Relative variation of total and static pressures and mass flows at stations 13 and 23 between two consecutive PROOSIS-CEDRE iterations  $\Delta_{i+1,i}$

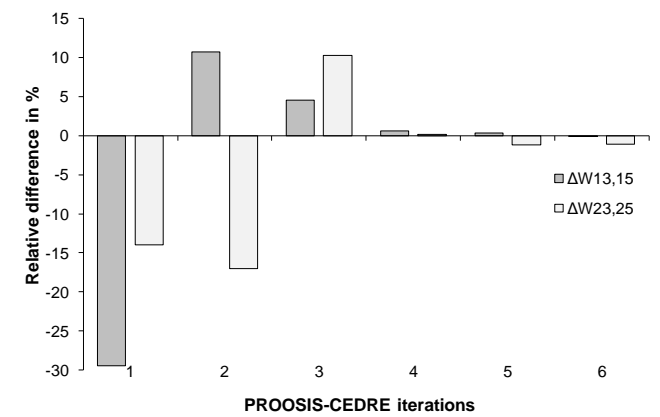


Figure 19 : Relative variation of mass flows between stations 13 and 15, and 23 and 25 respectively, at the end of each PROOSIS-CEDRE iteration

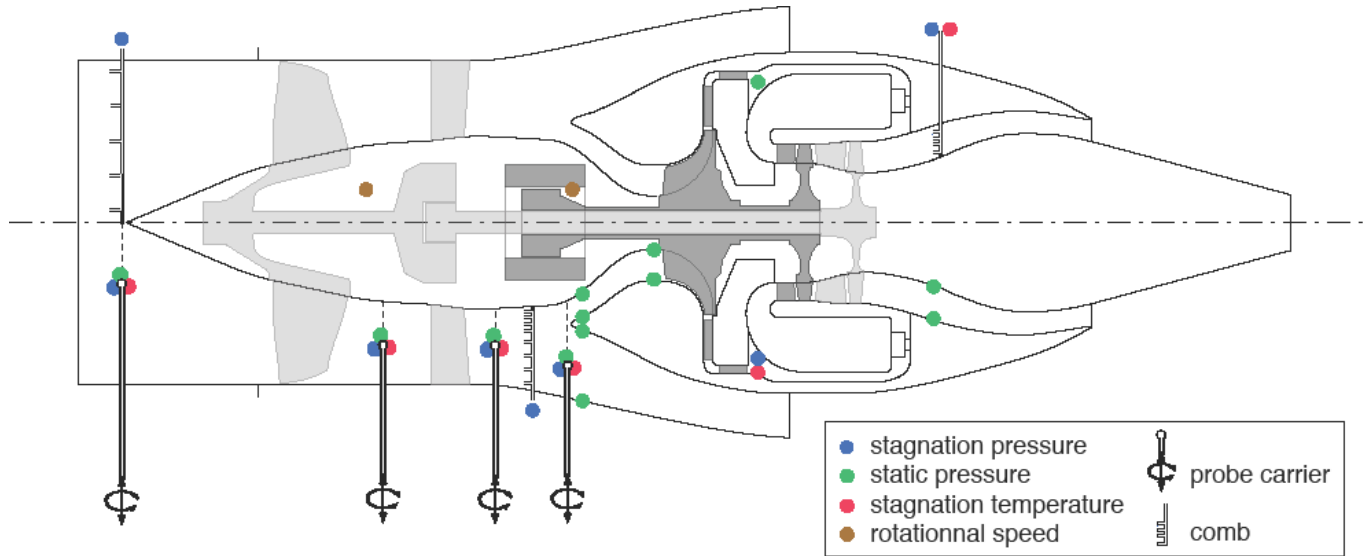


Figure 20: test rig on the DGEN380 bench at ISAE Propulsion lab